Hindawi Publishing Corporation
Journal of Sensors
Volume 2016, Article ID 5298197, 8 pages
http://dx.doi.org/10.1155/2016/5298197

Research Article

A Two-Dimensional CMUT Linear Array for Underwater Applications: Directivity Analysis and Design Optimization

Wen Zhang, Hui Zhang, Shijiu Jin, and Zhoumo Zeng

State Key Laboratory of Precision Measurement Technology and Instrument, Tianjin University, Tianjin 300072, China

Correspondence should be addressed to Hui Zhang; hzhang@tju.edu.cn

Received 12 February 2016; Accepted 24 March 2016

Academic Editor: Rui Tang

Capacitive micromachined ultrasonic transducers (CMUTs) are one of the promising MEMS devices. This paper proposed an integrated vibration membrane structure to design a two-dimensional CMUT linear array for underwater applications. The operation frequencies for different medium have been calculated and simulated, which are 2.5 MHz in air and 0.7 MHz in water. The directivity analyses for the CMUT cell, subarray, and linear array have been provided. According to the product theorems, the directivity function of the complex array is obtained using a combination of the directivity functions of certain simple structures. Results show that the directivity of a CMUT cell is weak due to the small size, but the directivity of the designed linear array is very strong. Influential parameters of the linear array have been discussed, including the cell numbers, the adjacent distance, and the operation medium. In order to further suppress the side lobe interference and improve the resolution and the imaging quality of the imaging system, several weighting methods are used for optimization and comparison. Satisfactory side lobe suppression results are obtained, which can meet the actual requirements.

1. Introduction

As the crucial component to achieve the conversion between acoustic energy and electrical energy, ultrasonic transducers are widely used in medical imaging, nondestructive evaluation, flow measurement, environmental chemical detection, and so on. Compared to traditional transducers, micromachined ultrasonic transducer (MUT) fabricated by microelectromechanical systems (MEMS) technology has great advantages in integration, which can structure system-in package (SIP) and even system-on chip (SOC) technologies [1]. Moreover, the MEMS technology controls the accuracy in micrometer (μm) magnitude, which largely reduces the fabrication errors and improves the consistency between arrays. Also, MEMS technology utilizes the silicon piezoresistivity or capacitance change to achieve the detection of acoustic signals, so the imaging resolution can be improved, too [2].

Currently, the MUT family includes capacitive micromachined ultrasonic transducers (CMUTs) based on flexural vibrations caused by a field-induced electrostatic attraction between suspended membrane and the substrate [3] and piezoelectric micromachined ultrasonic transducers (PMUTs) based on flexural vibrations caused by d_{31}-mode or d_{33}-mode excitation of a piezoelectric membrane [4, 5].

PMUT is made of a vibration membrane and piezoelectric thin film with the upper and lower electrodes. PMUTs do not require a large voltage bias and have fewer geometric and design constraints, facilitating integration with low voltage electronics. However, PMUT's impedance cannot match the acoustic impedance of air or fluid medium, so a surface matching layer is of great need for a better performance. Also, the high sensitivity of the resonant frequency to the residual stress of the PMUT membrane may cause difficulties during the design process. Residual stresses, which are a consequence of the various thermal treatments encountered during the fabrication process, are expected to result in an increased resonance frequency of the membrane if they were tensile in nature. The level of residual stresses in the layers is very dependent on the particular fabrication process and the processing conditions and is generally difficult to model [6].

Recently, CMUTs have been developed as a promising candidate for ultrasound transducer arrays for underwater application. Unlike PMUTs, the ultrasonic emission of CMUT is caused by the vibration of a very thin film,

which lowers CMUT's impedance to the same level of the surroundings. So the defects of PMUT impedance mismatch can be improved without adding the surface matching layer. CMUT based on MEMS technology is of small size, low noise, and wide operating temperature range. Therefore, predrive circuit, preamplifier, and signal processing circuits can be integrated on the same silicon wafer. Also, CMUTs have been demonstrated to produce fractional immersion bandwidth as wide as 175% and electromechanical coupling coefficient as high as 85%, which are better than conventional transducers [7]. In this paper, a two-dimensional MUT linear array consisting of CMUT cells is of research interest.

In 1996, Haller and Khuri-Yakub from Stanford University used surface micromachined technology and produced a microcapacitive ultrasonic transducer [8]. In 1999, they developed air-coupled nondestructive evaluation using micromachined ultrasonic transducers [9]. In 2002, Oralkan et al. from Stanford University developed a linear CMUT array and a 2D CMUT array which could implement 3D ultrasonic imaging [10, 11] and also conducted preliminary simulation experiments on imaging [12, 13]. In 2006, Caronti et al. developed a one-dimensional array of ultrasonic transducers and detectors used in medical ultrasonic imaging [14]. In China, Tianjin University was the first research group and they launched a research program using a CMUT array as the imaging and nondestructive detecting planar array [2, 15]. The Institute of Acoustics, Chinese Academy of Sciences, developed a microcapacitive microphone of circular structure [16]. The North University of China studied the method of designing MEMS capacitive ultrasonic transducer based on silicon wafer bonding process [17]. However, all these designs and research mentioned above did not involve actual applications of the device, and the finite element analysis is time-consuming. Therefore, carrying out research into CMUT design, simulation, and application helps to promote the development of CMUT and improvement of related technologies, which is of great research value and practical significance.

The arrangement optimization of a transducer array has been carried out to improve the radiated sound field directivity. Steinberg studied the focusing properties of uniform linear array composed of many point sources and ignores the array size and element number [18]. Wooh and Shi studied the linear array focusing effect, where the element length is infinite or the element length is much larger than the element width [19]. Actually, the element of a transducer array has certain size, and the array could have good effect of the spatial resolution with proper design. Compared with traditional one-dimensional linear array, the side leaking energy is more serious in the MEMS transducer array for smaller ratio of length to width. Therefore, the study on the directivity performance of the CMUT transducer array is very necessary.

Our aim is to analyze and optimize the directivity characteristics of CMUT cell and linear array, which would be accurate enough for designing and avoid massive finite element modeling. In this paper, Section 1 summarizes the development of the transducer community and issues the possibility of CMUT cell being a MEMS linear array for underwater application. Details of the main problems with former research are provided. Section 2 describes the geometry design of both CMUT cell and the two-dimensional linear array. The operation frequencies in different mediums are provided and proved by COMSOL Multiphysics software. Section 3 provides the directivity analysis for CMUT cell, subarray, and two-dimensional linear array. The directivity function of the complex array is obtained using the product theorems. Section 4 makes further discussion and optimization for CMUT subarray and two-dimensional array. Different influential parameters are considered for design and modeling. Side lobe suppression methods are compared and discussed. Section 5 concludes the paper and assesses the regime of validity of the present analysis.

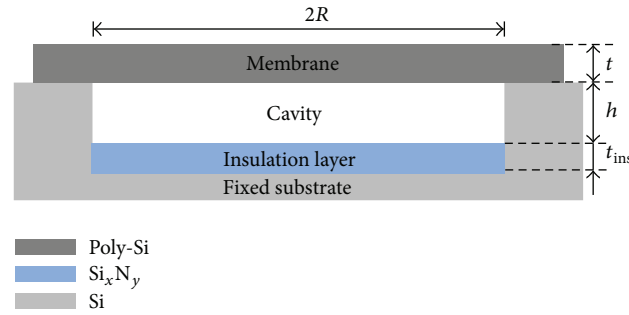

Figure 1: Geometry of a flat circular CMUT cell.

2. Geometry Design of CMUT Cell and Linear Array

A CMUT cell is built with a circular, square, or hexagonal membrane separated from a fixed substrate by a small airgap [2, 20]. The geometry of the circular CMUT cell is shown in Figure 1. The vibrating membrane of the CMUT cell is made from a conducting ploysilicon membrane [21]. A layer of silicon dioxide is deposited in order to prevent the electrical shortcut between the two electrodes. The highly doped silicon substrate is also utilized as the bottom electrode.

Determination of the array resonant frequency has a significant influence on the array design and optimization. The CMUT often generates or detects ultrasonic waves by the vibrating membrane featuring fixed circumference. Then the resonant frequency of a clamped circular microplate in vacuum can be calculated as [22, 23]

$$f_0 = 0.467 \frac{t}{R^2} \sqrt{\frac{E}{\rho\left(1-\sigma^2\right)}}, \tag{1}$$

where t and R are the membrane thickness and radius, respectively. E is Young's modulus, ρ is the membrane density, and σ is Poisson's ratio.

When the CMUT cell is working for underwater applications, the influence of the surrounding medium cannot

Table 1: Material properties of the CMUT (20°C).

	Poly-Si	SiN_x	SiO_2	Water
Young's modulus/GPa	160	320	70	—
Density/g/cm^3	2.32	3.27	2.2	0.9982
Poisson's ratio	0.22	0.26	0.17	—
Relative permittivity	4.5	5.7	4.2	—

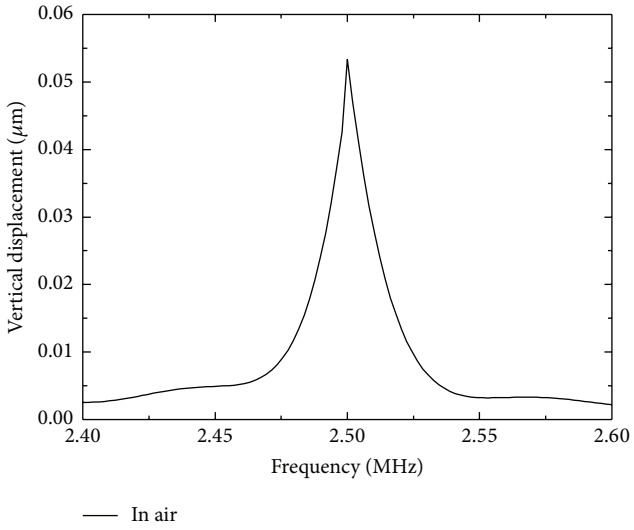

Figure 2: Harmonic analysis for a CMUT cell in air.

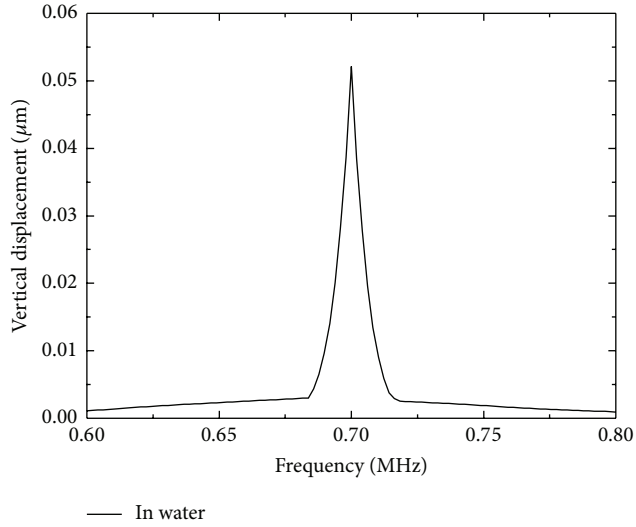

Figure 3: Harmonic analysis for a CMUT cell in water.

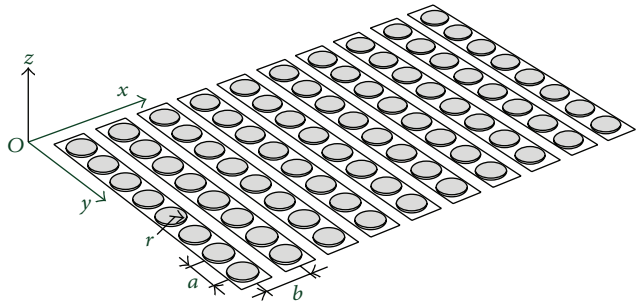

Figure 4: Geometry of a two-dimensional CMUT linear array.

be ignored. Due to the effect of the medium, the resonant frequency in water can be expressed as [23, 24]

$$f_l = \frac{1}{\sqrt{1 + 0.67\rho_l R/\rho t}} f_0, \tag{2}$$

where ρ_l represents the density of the surrounding liquid.

In our case, the membrane radius R is 40 μm and the thickness t is 1 μm. Relevant material properties used in theory analysis are summarized in Table 1. The resonant frequency of transducer is calculated as 2.49 MHz in vacuum and 0.71 MHz in water.

The resonant frequencies of the transducer with the same structure parameters for airborne and underwater applications are also analyzed by finite element method and the results are compared with (1) and (2). As shown in Figures 2 and 3, the results of the harmonic analysis simulated by the COMSOL Multiphysics software are 2.50 MHz and 0.7 MHz, which are consistent with the theoretical analysis of a clamped circular plate. For the same geometry, the CMUT cell shows a lower operation frequency for underwater applications. In our work, (1)~(2) and COMSOL simulations are adopted to more accurately predict the array resonant frequencies for different applications.

In order to increase radiation sound pressure of the two-dimensional CMUT linear array, we designed an array structure based on CMUT with the circular membrane. As shown in Figure 4, the M CMUT cells in subarray are arranged by parallel connection, where a and r are the intercell spacing and the cell radius. The N subarrays are uniformly arranged in Oxy plane, and the distance between two adjacent subarrays is b.

3. Directivity Analysis for CMUT Linear Array

The directivity is a crucial parameter for CMUT design, and it describes that the amplitude of its transmitting response or receiving response is varying with an azimuth, which is also a kind of attribute in the far field. This is usually evaluated by using the directivity function, directivity diagram, beam width, side lobe level, and so on.

The following analyses assume that the subarray or the two-dimensional array is located along the x-axis, which is in Oxy plane of three-dimensional space coordinate system as shown in Figure 4, and its surface points to the Oxz plane.

The normalized directivity function can be expressed as

$$D(\alpha, \theta) = \left| \frac{P(\alpha, \theta)}{P(\alpha_m, \theta_m)} \right|, \tag{3}$$

where α and θ are the standard spherical coordinate angles. $P(\alpha, \theta)$ is the sound pressure of the arbitrary position (α, θ)

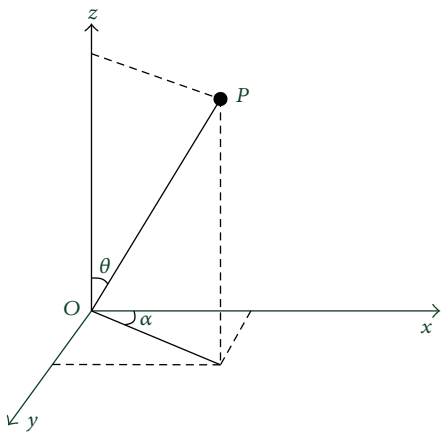

Figure 5: Schematic for directivity analysis using normalized sound pressure.

in the far field, and $P(\alpha_m, \theta_m)$ is the biggest sound pressure, as shown in Figure 5.

The directivity function of the complex array is generally simplified as a combination of the directivity functions of certain simple structures. Using the Bridge product theorems, the complex array directivity function can be obtained by taking the product of the directivity function of the simple structures.

For the two-dimensional CMUT linear array shown in Figure 4, the radiated sound field directivity function is equal to the product of a single subarray directivity function and a linear array directivity function composed of N point sources in each element center.

The CMUT cell as shown in Figure 1 can be taken as a single circular piston with radius r, and the directivity function of the circular piston in the Oxz plane is

$$D_c(\theta) = \left| \frac{2J_1(kr\sin\theta)}{kr\sin\theta} \right|, \tag{4}$$

where k is the wave number, r is the radius, θ is the angle between the acoustic line and the z-axis, and $J_1(x)$ is the first-order Bessel function.

According to the Bridge product theorem, a CMUT linear subarray can be regarded as a rectangular piston, and in the Oxz plane its directivity function is

$$D_s(\alpha, \theta, \alpha_m, \theta_m) = \left| \frac{\sin\left[(kMa/2)\left(\cos\alpha\sin\theta - \cos\alpha_m\sin\theta_m\right)\right]}{M\sin\left[(ka/2)\left(\cos\alpha\sin\theta - \cos\alpha_m\sin\theta_m\right)\right]} \right|. \tag{5}$$

Considering the uniform linear array composed of N point sources, each subarray has the same resonant frequency, the vibration amplitude, and the phase. Multiplication manipulation using (3)~(5) leads to the following expression for the sound pressure normalized directivity function:

$$D_a(\alpha, \theta, \alpha_m, \theta_m) = \left| \frac{2J_1(kr\sin\theta)}{kr\sin\theta} \cdot \frac{\sin\left[(kMa/2)\left(\cos\alpha\sin\theta - \cos\alpha_m\sin\theta_m\right)\right]}{M\sin\left[(ka/2)\left(\cos\alpha\sin\theta - \cos\alpha_m\sin\theta_m\right)\right]} \cdot \frac{\sin\left[(kNb/2)\left(\cos\alpha\sin\theta - \cos\alpha_m\sin\theta_m\right)\right]}{N\sin\left[(kb/2)\left(\cos\alpha\sin\theta - \cos\alpha_m\sin\theta_m\right)\right]} \right|. \tag{6}$$

4. Discussion and Optimization

In order to improve the imaging resolution and imaging quality in an ultrasonic imaging system, one-dimensional or two-dimensional linear array ultrasonic transducer is often used to implement the ultrasonic imaging. The sound beam that the CMUT array radiated to the three-dimensional space will produce a relative maximum amplitude of the sound pressure in a steering angle direction. If the designed parameters are not optimized, the radiation of the sound beam will tend to produce the grating lobes and side lobes around the main lobe. The existence of the grating lobes and the side lobes means the sound waves propagate in other directions, which causes the "leakage" of the beam energy and affects the signal-to-noise ratio of the system. Besides, a strong side lobe inhibits the ability of the array to detect a weaker signal in the presence of a larger nearby signal. Thus, the array parameters should be discussed and optimized by minimizing the main lobe width, eliminating grating lobes, and suppressing side lobes as much as possible.

4.1. CMUT Subarray Optimization. To discuss the directivity of a CMUT subarray, many parameters have to be considered. For a CMUT subarray composed of M cells as in Figure 3, the operation frequency of the CMUT linear array is designed to be 0.71 MHz for underwater application, and the sound velocity in water is 1540 m/s, so the wavelength can be calculated as

$$\lambda = \frac{v_l}{f_l} = \frac{1540\ \text{m/s}}{0.71\ \text{MHz}} \approx 2169\ \mu\text{m}. \tag{7}$$

To avoid the grating lobes, the distance between two adjacent cells in one subarray is supposed to be no more than 0.5λ. Consider the distance between two adjacent cells for our analysis to be 0.5λ. When the azimuth angle is 0° and there is no steering, the directivity of a subarray varies with different cell number M, as shown in Figure 6.

From Figure 6, it can be seen that when the cell number increases, the main lobe width decreases, indicating a better resolution and a more sensitive receiving angle range. Also, with more cells in one subarray, the amplitude of the side lobes decreases. For more than 16 cells in one subarray, the main lobe width slightly decreases, unlike the obvious decrease from $M = 4$ to $M = 8$. So, for the following analysis, 16 cells linearly arranged in one subarray have been chosen.

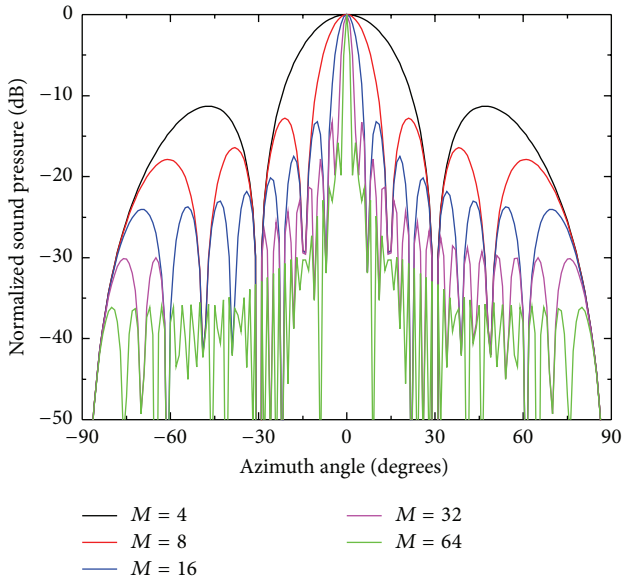

Figure 6: Directivity analysis with different cell number in a subarray.

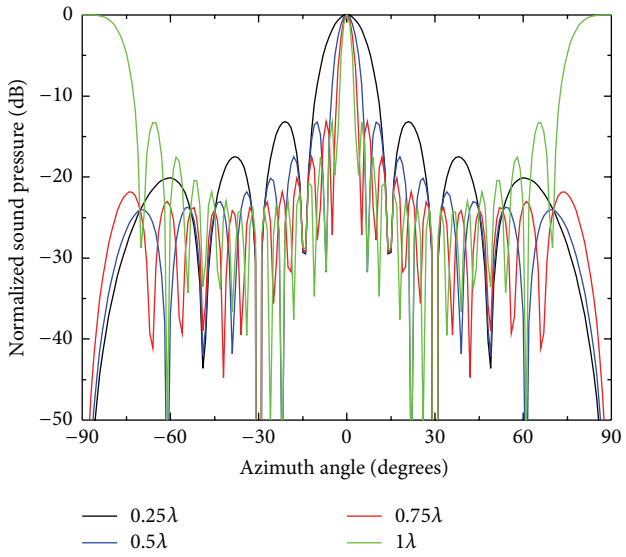

Figure 7: Directivity analysis with different distance between adjacent cells.

When the azimuth angle is 0° and there is no steering, the directivity of a 16-cell subarray varies with different distance between two adjacent cells, as shown in Figure 7.

From Figure 7, it can be noticed that when the distance between two adjacent cells in a subarray increases, the main lobe width decreases. However, increasing the adjacent distance can also arouse grating lobes, such as in the 1λ case. Take both the main lobe width and the grating lobes into consideration; the adjacent distance 0.5λ is preferred for the following analysis.

The operation medium also has big influence on the directivity performance of the CMUT linear subarray. The distance between two adjacent cells is set to be 1085 μm,

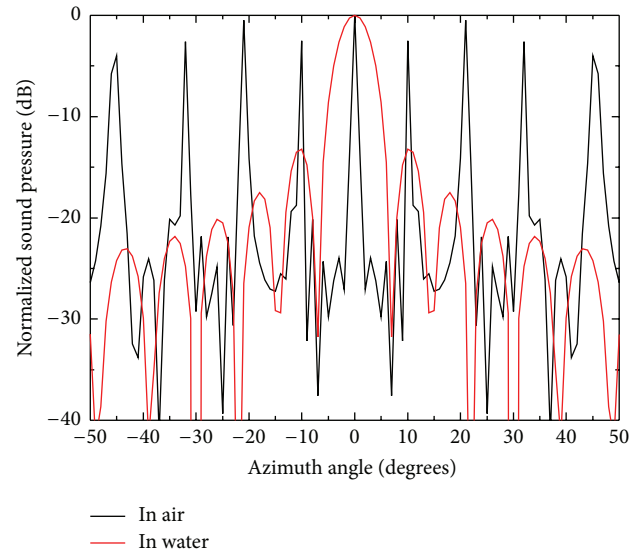

Figure 8: Directivity analysis with different operation medium.

which is 0.5λ for underwater applications. When the same array is operated in air, the directivity performance is different, as shown in Figure 8.

From Figure 8, it can be observed that, for different operation medium, directivity performances are different. For the same cell dimensions, subarray geometry, and adjacent distance, the grating lobes appear for airborne applications. The sound velocity in air is about 340 m/s, and the operation frequency is 2.5 MHz, so the wavelength in air can be expressed as

$$\lambda_{\text{air}} = \frac{v_{\text{air}}}{f_0} = \frac{340\ \text{m/s}}{2.5\ \text{MHz}} = 136\ \mu\text{m}. \quad (8)$$

Compared to the wavelength in water (1540 μm), the wavelength in air is much smaller. From Figure 7, it can be obtained that when the distance between two adjacent cells is bigger than wavelength, there will be grating lobes. In this case, the adjacent distance is 1085 μm, which is much bigger than the wavelength in air. So the grating lobes appear and the energy leakage increases, which also proves that a CMUT linear array for underwater applications may not be suitable for airborne applications without modification and optimization.

From Figures 6–8, several influential parameters have been discussed, including the cell numbers, the adjacent distance, and the operation medium. During the design phase of a CMUT array, these parameters have to be considered for better and more stable performance.

4.2. Two-Dimensional CMUT Linear Array Optimization. A disadvantage of the CMUT linear subarray is its large side lobes. A strong side lobe inhibits the ability of the array to detect a weaker signal in the presence of a larger nearby signal. In this section, the two-dimensional CMUT linear array consisting of 16×8 cells (Figure 4) is chosen for analysis.

Tapering functions can be used to suppress the side lobes, and the generalized cosine windows are one of the

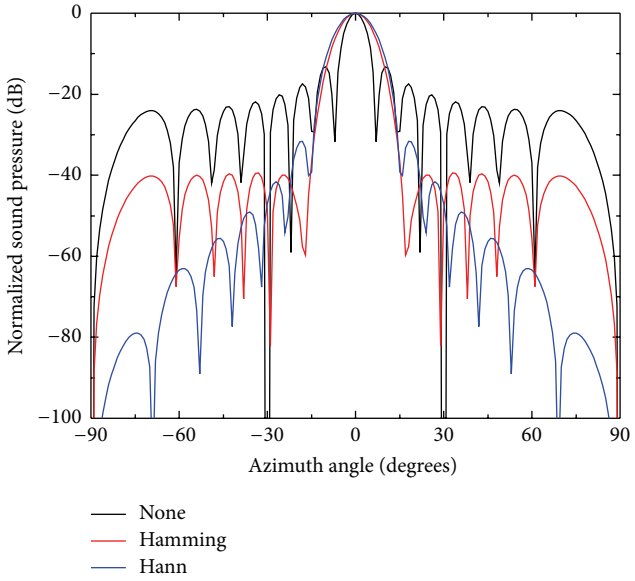

Figure 9: Directivity analyses before and after the Hann/Hamming methods.

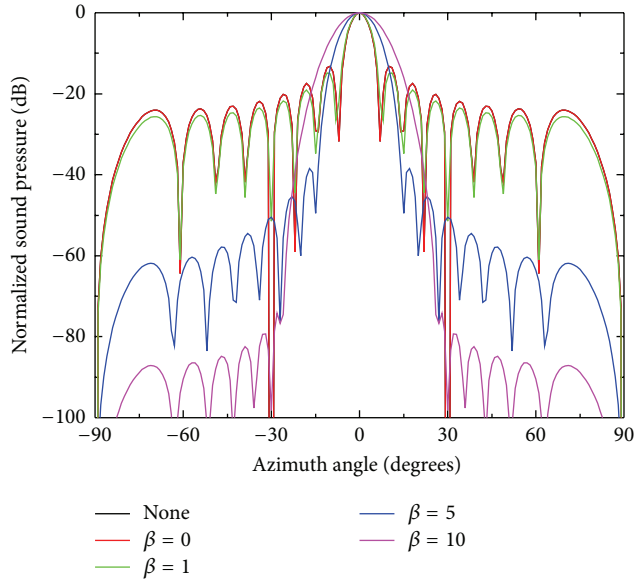

Figure 10: Directivity analyses before and after the Kaiser method.

most common methods, including the Hann window and the Hamming window. The mathematical expression of the Hann window is

$$w(m) = \frac{1}{2}\left[1 - \cos\left(\frac{2\pi m}{M}\right)\right] \quad 0 \le m \le M \tag{9}$$

and the Hamming window expression is

$$w(m) = 0.54 - 0.46\cos\left(\frac{2\pi m}{M}\right) \quad 0 \le m \le M, \tag{10}$$

where M represents the cell number.

Directivity analyses before and after the generalized cosine methods are shown in Figure 9. Results show that both Hamming and Hann methods can decrease the side lobe amplitude, but both at the expense of broadening the main lobe width. The two methods are quite similar, and the Hann method appears to have a faster decreasing rate.

Another side lobe suppression method is the Kaiser window weighting method, and the mathematical expression is

$$w(m) = \frac{I_0\left[\beta\sqrt{1-(1-2m/M)^2}\right]}{I_0(\beta)} \quad 0 \le m \le M, \tag{11}$$

where $I_0(x)$ is the zero-order modified Bessel function. β is the shape function with relation to the side lobe amplitude p_s, and the expression is

$$\beta = \begin{cases} 0.1102\,(p_s - 8.7) & p_s > 50 \\ 0.5482\,(p_s - 21)^{0.4} + 0.07886\,(p_s - 21) & 21 \le p_s \le 50 \\ 0 & p_s < 21. \end{cases} \tag{12}$$

For different β values, the directivity performances are different, as shown in Figure 10. When $\beta = 0$, the directivity performance after the Kaiser weighting method remains the same as before. When β increases, the side lobe amplitude decreases, also at the expense of broadening the main lobe width. Compared to other weighting methods, the ratio of the main lobe energy to the side lobe energy of the Kaiser method is almost the biggest. Besides, the main lobe width and the side lobe amplitude can be freely regulated for different applications.

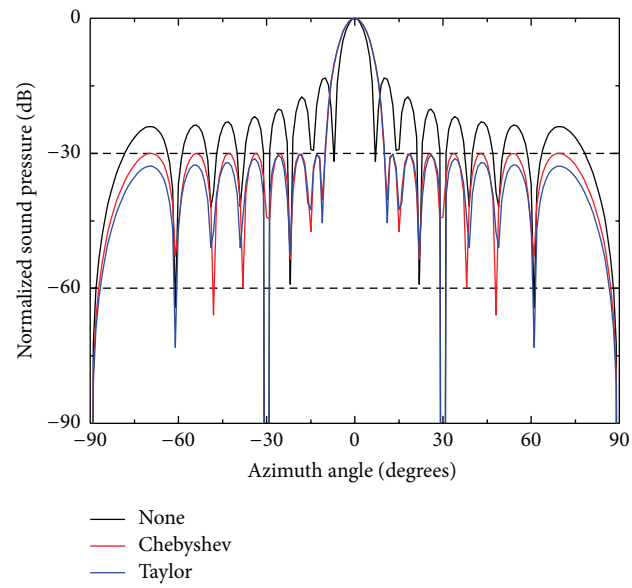

Figure 11: Directivity analyses before and after the Chebyshev/Taylor methods.

Besides, the Chebyshev and Taylor weighting methods are also chosen for comparison. The −30 dB side lobe suppressions are carried out using the two methods, and the directivity performances are shown in Figure 11.

From Figure 11, it can be observed that the Taylor method is similar to the Chebyshev method. Both methods have decreased the side lobe amplitude to around −30 dB, and the main lobe width has been broadened. Whereas the Chebyshev method has the narrowest possible main lobe for a specified side lobe level, the Taylor method offers tradeoffs between the main lobe width and the side lobe level. Moreover, the Taylor distribution avoids edge discontinuities, so the Taylor method side lobes decrease monotonically.

From Figures 9–11, several common side lobe suppression methods have been discussed and compared. Since the main lobe width and the side lobe amplitude are contradictory, the side lobe suppression method must be carefully chosen due to different design requirements. For instance, when high lateral resolutions are desired, the main lobe width is the first concern. When the signal-to-noise ratio is the important requirement, the side lobe level is the first concern.

5. Conclusion

This paper proposed an integrated vibration membrane structure to design a CMUT linear array consisting of many subarrays for underwater applications. The directivity performances and side lobe suppression methods have been discussed. The work in this paper is summarized as follows.

(1) A two-dimensional CMUT linear array for underwater applications has been proposed. The operation frequencies for different medium have been calculated, which are also proved by the COMSOL Multiphysics software. The derivation takes the ambient fluid into consideration, and the operation frequency of the CMUT cell is 2.5 MHz in air and 0.7 MHz in water.

(2) The directivity analyses for the CMUT cell, subarray, and two-dimensional linear array have been provided. The directivity of a single circular CMUT cell is very weak, so it should be composed into linear array to enhance the directivity. According to the product theorems, the directivity function of the complex array is obtained using a combination of the directivity functions of certain simple structures.

(3) The effects of the correlation parameters of the linear subarray have been discussed, including the cell numbers, the adjacent distance, and the operation medium. Results show that both the cell numbers and the adjacent distance have effect on the main lobe width. However, both of them have an upper limit in order to eliminate grating lobes. For the underwater applications, the wavelength is much bigger than that for the airborne applications. Thus, the directivity performance of a linear subarray is determined by several parameters simultaneously.

(4) In order to reduce the side lobe of the CMUT linear array, several weighting methods are used to suppress the side lobe amplitude, which is quite satisfactory, but at the expense of broadening the main lobe width. Since the main lobe width and the side lobe amplitude are contradictory, the side lobe suppression method must be carefully chosen due to different design requirements, and the imaging quality and resolution of the imaging system can be improved further.

Competing Interests

The authors declare that they have no competing interests.

Acknowledgments

This work has been supported by the Young Scientists Fund of the National Natural Science Foundation of China (Grant no. 61201039).

References

[1] Y. Qiu, J. V. Gigliotti, M. Wallace et al., "Piezoelectric micromachined ultrasound transducer (PMUT) arrays for integrated sensing, actuation and imaging," *Sensors*, vol. 15, no. 4, pp. 8020–8041, 2015.

[2] W. Zhang, H. Zhang, F. Du, J. Shi, S. Jin, and Z. Zeng, "Pull-in analysis of the flat circular CMUT cell featuring sealed cavity," *Mathematical Problems in Engineering*, vol. 2015, Article ID 150279, 9 pages, 2015.

[3] Ö. Oralkan, A. S. Ergun, J. A. Johnson et al., "Capacitive micromachined ultrasonic transducers: next generation arrays for acoustic imaging?" *IEEE Transactions on Ultrasonics, Ferroelectrics, and Frequency Control*, vol. 49, no. 11, pp. 1596–1610, 2002.

[4] D. E. Dausch, J. B. Castellucci, D. R. Chou, and O. T. von Ramm, "Theory and operation of 2-D array piezoelectric micromachined ultrasound transducers," *IEEE Transactions on Ultrasonics, Ferroelectrics, and Frequency Control*, vol. 55, no. 11, pp. 2484–2492, 2008.

[5] A. Hajati, D. Latev, D. Gardner et al., "Three-dimensional micro electromechanical system piezoelectric ultrasound transducer," *Applied Physics Letters*, vol. 101, no. 25, Article ID 253101, 2012.

[6] F. Akasheh, J. D. Fraser, S. Bose, and A. Bandyopadhyay, "Piezoelectric micromachined ultrasonic transducers: modeling the influence of structural parameters on device performance," *IEEE Transactions on Ultrasonics, Ferroelectrics, and Frequency Control*, vol. 52, no. 3, pp. 455–468, 2005.

[7] A. S. Ergun, C.-H. Cheng, O. Oralkan et al., "Broadband capacitive micromachined ultrasonic transducers ranging from 10 kHz to 60 MHz for imaging arrays and more," in *Proceedings of the IEEE Ultrasonics Symposium*, pp. 1039–1043, Munich, Germany, October 2002.

[8] M. I. Haller and B. T. Khuri-Yakub, "A surface micromachined electrostatic ultrasonic air transducer," *IEEE Transactions on Ultrasonics, Ferroelectrics, and Frequency Control*, vol. 43, no. 1, pp. 1–6, 1996.

[9] S. T. Hansen, B. J. Mossawir, A. Sanli Ergun, F. Degertekin, and B. T. Khuri-Yakub, "Air-coupled nondestructive evaluation using micromachined ultrasonic transducers," in *Proceedings of the IEEE Ultrasonics Symposium*, pp. 1037–1040, Lake Tahoe, Nev, USA, October 1999.

[10] J. Johnson, Ö. Oralkan, U. Demirci, S. Ergun, M. Karaman, and P. Khuri-Yakub, "Medical imaging using capacitive micromachined ultrasonic transducer arrays," *Ultrasonics*, vol. 40, no. 1-8, pp. 471–476, 2002.

[11] X. Zhuang, A. S. Ergun, Y. Huang, I. O. Wygant, O. Oralkan, and B. T. Khuri-Yakub, "Integration of trench-isolated through-wafer interconnects with 2d capacitive micromachined ultrasonic transducer arrays," *Sensors and Actuators A: Physical*, vol. 138, no. 1, pp. 221–229, 2007.

[12] X. Zhuang, D.-S. Lin, Ö. Oralkan, and B. T. Khuri-Yakub, "Fabrication of flexible transducer arrays with through-wafer electrical interconnects based on trench refilling with PDMS," *Journal of Microelectromechanical Systems*, vol. 17, no. 2, pp. 446–452, 2008.

[13] I. O. Wygant, N. S. Jamal, H. J. Lee et al., "An integrated circuit with transmit beamforming flip-chip bonded to a 2-D CMUT array for 3-D ultrasound imaging," *IEEE Transactions on Ultrasonics, Ferroelectrics, and Frequency Control*, vol. 56, no. 10, pp. 2145–2156, 2009.

[14] A. Caronti, G. Caliano, R. Carotenuto et al., "Capacitive micromachined ultrasonic transducer (CMUT) arrays for medical imaging," *Microelectronics Journal*, vol. 37, no. 8, pp. 770–777, 2006.

[15] W. Zhang, H. Zhang, Y. Wang, F. Du, S. Jin, and Z. Zeng, "Simulation characterization of CMUT with vented square membrane," in *Proceedings of the International Conference on Optical Instrument and Technology (OIT '15)*, Beijing, China, May 2015.

[16] Z. H. Hao, L. Tang, and D. H. Qiao, "Analysis of the resonant frequency of capacitive micro-machined ultrasonic transducer (cMUT) with finite element method," *Technical Acoustics*, vol. 28, pp. 133–134, 2009 (Chinese).

[17] J. Miao, C. D. He, D. Q. Lian et al., "Design of MEMS capacitive ultrasonic transducer based on wafer bonding technology," *Chinese Journal of Sensors and Actuators*, vol. 25, no. 12, pp. 1653–1658, 2012 (Chinese).

[18] B. D. Steinberg, *Principles of Aperture and Array System Design: Including Random and Adaptive Arrays*, John Wiley & Sons, New York, NY, USA, 1976.

[19] S.-C. Wooh and Y. Shi, "Influence of phased array element size on beam steering behavior," *Ultrasonics*, vol. 36, no. 6, pp. 737–749, 1998.

[20] C. B. Doody, X. Cheng, C. A. Rich, D. F. Lemmerhirt, and R. D. White, "Modeling and characterization of CMOS-fabricated capacitive micromachined ultrasound transducers," *Journal of Microelectromechanical Systems*, vol. 20, no. 1, pp. 104–118, 2011.

[21] M. L. Kuntzman, D. Kim, and N. A. Hall, "Microfabrication and experimental evaluation of a rotational capacitive micromachined ultrasonic transducer," *Journal of Microelectromechanical Systems*, vol. 24, no. 2, pp. 404–413, 2015.

[22] M. Bao, *Analysis and Design Principles of MEMS Devices*, Elsevier, New York, NY, USA, 2005.

[23] M. R. Haddara and S. Cao, "A study of the dynamic response of submerged rectangular flat plates," *Marine Structures*, vol. 9, no. 10, pp. 913–933, 1996.

[24] X. H. Si, W. X. Lu, and F. L. Chu, "Modal analysis of circular plates with radial side cracks and in contact with water on one side based on the Rayleigh–Ritz method," *Journal of Sound and Vibration*, vol. 331, no. 1, pp. 231–251, 2012.